ELSEVIER

Journal of Power Sources 68 (1997) 604–608

JOURNAL OF POWER SOURCES

Preparation and electrochemical investigation of $LiMn_{2-x}Me_xO_4$ (Me: Ni, Fe, and $x=0.5, 1$) cathode materials for secondary lithium batteries

K. Amine *, H. Tukamoto, H. Yasuda, Y. Fujita

Fundamental Technology Laboratory, Corporate R&D Center, Japan Storage Battery Co., Ltd., Nishinosho, Kisshoin, Minami-ku, Kyoto 601, Japan

Accepted 14 October 1996

Abstract

The spinels $LiMn_{1.5}Me_{0.5}O_4$ and $LiMnMeO_4$ (Me: Ni, Fe) were prepared using either a sol–gel process in the case of nickel doping, or a solid-state reaction in the case of iron doping. X-ray diffraction analysis revealed differences in the patterns when the content of the dopant in the spinel increases. The pattern of $LiMn_{1.5}Ni_{0.5}O_4$ was indexed as a pure cubic spinel together with that of $LiMn_{1.5}Fe_{0.5}O_4$, whereas $LiMnNiO_4$ was found to be indexed mainly as a hexagonal layered phase since it was difficult to distinguish between these two structures because the diffraction peaks were broad. On the other hand, the pattern corresponding to $LiMnFeO_4$ was indexed as an inverse spinel. The material $LiMn_{1.5}Ni_{0.5}O_4$ could intercalate both chemically and electrochemically a second lithium at 3 V without structural changes and with a large discharge capacity of 160 mAh/g. This material presents also a 4.7 V plateau with 90 mAh/g capacity due to the oxidation of divalent nickel to the tetravalent state when first charged. A tetragonal phase due to the Jahn–Teller distortion was observed in the material $Li_{1+x}Mn_{1.5}Fe_{0.5}O_4$ with a discharge curve showing 4.1 and 2.9 V plateaus as in the case of the spinel $Li_xMn_2O_4$ ($0 \le x \le 2$) without doping. X-ray photoelectron spectroscopy has revealed that the nickel was divalent in $LiMn_{1.5}Ni_{0.5}O_4$ and trivalent in $LiMnNiO_4$, whereas, iron was trivalent in both $LiMn_{1.5}Fe_{0.5}O_4$ and $LiMnFeO_4$. The structure and the electrochemical behavior of the above materials were investigated and correlated with the oxidation state of the dopants

Keywords: Lithium batteries; Cathode materials; Manganese; Nickel; Iron

1. Introduction

The spinel $LiMn_2O_4$ is currently a strong potential candidate for future application as the cathode material for lithium secondary batteries [1–3]. This material is known to intercalate reversibly two lithium atoms at 4 and 3 V generating, thus, a large capacity of 308 mAh/g [4,5]. This capacity is, however, offset by the potential drop from 4 to 3 V versus Li/Li^+ which occurs during both the charge and the discharge processes. In this case, the average manganese ion valence falls below 3.5, and a strong Jahn–Teller distortion is introduced into the spinel structure, thus reducing its crystal symmetry from cubic to tetragonal. To combat the onset of the Jahn–Teller effect, one should investigate the replacement of manganese with an extensive amount of a low valence 3d metal. Several groups have already studied the effect of limited substitution of manganese with different valence metals such as Ni, Co, Zn, Fe [6,7]. In these cases, no significant improvement in cell capacity at 4 V versus Li/Li^+, nor any substantial decrease in potential drop from 4 to 3 V was observed. Other authors [8] adopted the approach of increasing the average manganese ion valence slightly above 3.5 by replacing some manganese with lithium ($Li_{1+\delta}Mn_{2-\delta}O_4$) or by preparing cation defect spinels of the composition $Li_{1-\delta}Mn_{2-2\delta}O_4$. In this paper, we studied the effect of nickel and iron substitution on the electrochemical performance of $LiMn_{1.5}Me_{0.5}O_4$ and $LiMnMeO_4$ (Me: Ni, Fe) materials.

2. Experimental

The low-temperature sol–gel process was used for the extensive doping of the spinel with nickel because of the difficulty observed when using the solid-state reaction [9]. Spinel $LiMn_{1.5}Me_{0.5}O_4$ (Me: Ni, Fe) and $LiMnNiO_4$ were prepared using as precursors: manganese acetate, lithium nitrate and nickel acetate or iron lactate. The precursors were first dissolved in distilled water before an excess of ammonia

* Corresponding author.

PII S0378-7753(96)02590-6

was added to give a precipitate. A small amount of carbon black or gelatin was used as the stabilizing agent. The viscous precipitates were partially dried, coated on titanium foil and then calcined in air at 300 °C. The material $LiMnFeO_4$ was prepared by the solid-state reaction at a very high temperature. γ-MnO_2, $LiNO_3$ and γ-Fe_2O_3 were first mixed, strongly ground and then calcined in air at 1150 °C.

3. Structure and oxidation state of dopant

Fig. 1 (a) and (c) shows the X-ray diffraction (XRD) patterns of $LiMn_{1.5}Ni_{0.5}O_4$ and $LiMn_{1.5}Fe_{0.5}O_4$. Both materials exhibit a cubic spinel structure with a unit cell parameter of $a = 8.176$ Å and $a = 8.190$ Å, respectively. The patterns present broad peaks indicating that both materials have a large surface area as shown by BET which gave a specific surface area of 12.9 and 11.3 m^2/g for $LiMn_{1.5}Ni_{0.5}O_4$ and $LiMn_{1.5}Fe_{0.5}O_4$, respectively. The obtained materials were then chemically lithiated using either an excess of LiI dissolved in acetonitrile solvent at 80 °C for $LiMn_{1.5}Ni_{0.5}O_4$ and *n*-butyllithium dissolved in hexane for $LiMn_{1.5}Fe_{0.5}O_4$, because LiI reacts with iron in the spinel leading to the formation of FeI_2. Ion chromatography and atomic absorption analyses of nickel-doped material gave an average composition of $Li_{2.02}Mn_{1.56}Ni_{0.52}O_4$ by XRD (Fig. 1(b)) similar to the spinel starting compound. This result is in contrast to that of $LiMn_2O_4$, without nickel doping, where a structural transition from cubic to tetragonal occurred after the formation of $Li_2Mn_2O_4$. In the case of the iron-doped spinel, the chemical lithiation was partial ($Li_{1.47}Mn_{1.5}Fe_{0.5}O_4$) and resulted in the formation of a tetragonal phase denoted by (*) mixed

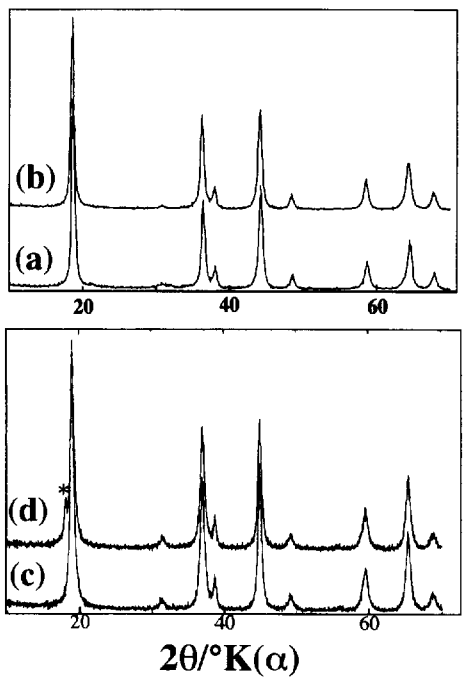

Fig. 1. XRD patterns of: (a) $LiMn_{1.5}Ni_{0.5}O_4$; (b) $Li_2Mn_{1.5}Ni_{0.5}O_4$; (c) $LiMn_{1.5}Fe_{0.5}O_4$, and (d) $Li_{1.47}Mn_{1.5}Fe_{0.5}O_4$.

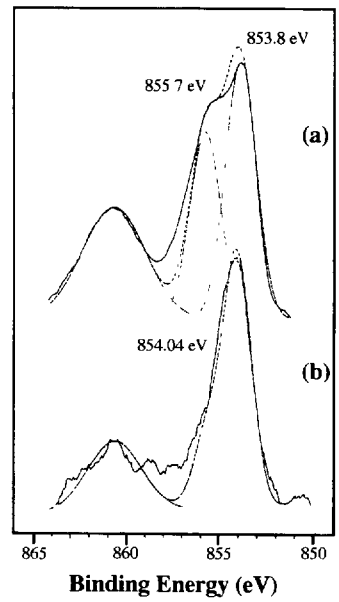

Fig. 2. XPS $Ni2p_{3/2}$ emission spectra of: (a) NiO, and (b) $LiMn_{1.5}Ni_{0.5}O_4$.

with a spinel phase. In this case only the most intense peak is observed because the amount of tetragonal phase is very small. The oxidation state of nickel and iron dopants was studied by X-ray photoelectron spectroscopy (XPS). The $Ni2p_{3/2}$ emission spectrum of $LiMn_{1.5}Ni_{0.5}O_4$ (Fig. 2(b)) shows one sharp peak at low binding energy associated with a broad satellite peak. The binding energy of this peak (854.04 eV) is very close to that observed in the low binding energy of the NiO (Fig. 2(a)) and falls within the range of those reported in divalent nickel-based materials [10]. The high binding energy observed in the NiO spectrum corresponds to trivalent nickel due to impurities in the material. The XPS results indicate that no Jahn–Teller effect could take place because the initial oxidation state of manganese in $LiMn_{1.5}Ni_{0.5}O_4$ is tetravalent. Fig. 3(b) shows the $Fe2p_{3/2}$

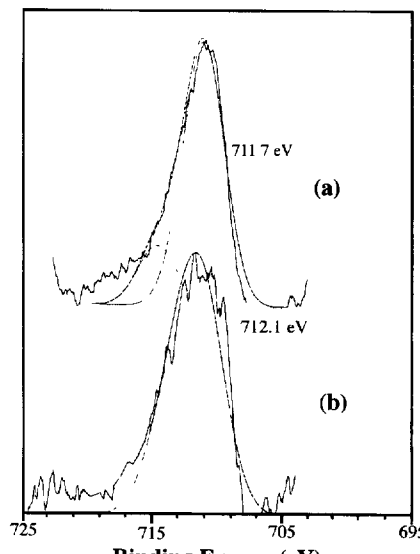

Fig 3. XPS $Fe2p_{3/2}$ emission spectra of: (a) Fe_2O_3, and (b) $LiMn_{1.5}Fe_{0.5}O_4$.

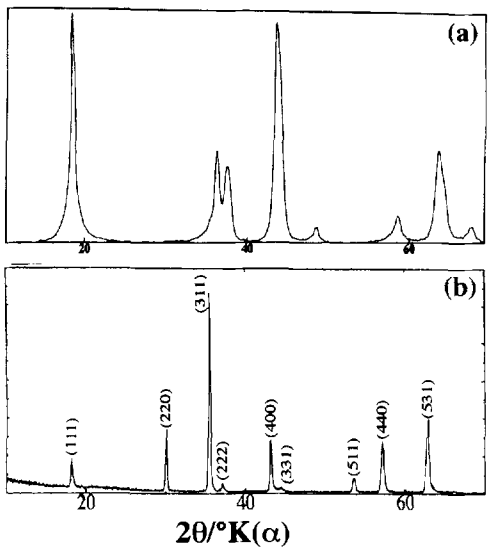

Fig. 4. XRD patterns of: (a) $LiMnNiO_4$, and (b) $LiMnFeO_4$.

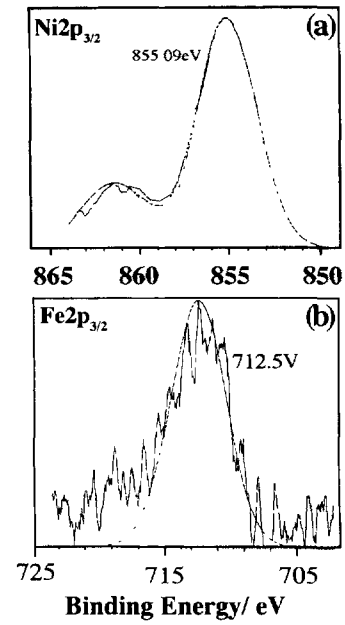

Fig 5 XPS spectra of: (a) $Ni2p_{3/2}$ emission of $LiMnNiO_4$, and (b) $Fe2p_{3/2}$ emission of $LiMnFeO_4$

emission spectrum of $LiMn_{1.5}Fe_{0.5}O_4$. The material presents also one peak at a binding energy (712.1 eV) very close to that observed in Fe_2O_3 (Fig. 3(a)) revealing, thus, the (3+) oxidation state of iron in contrast to divalent nickel in $LiMn_{1.5}Ni_{0.5}O_4$. The trivalent state of iron in $LiMn_{1.5}Fe_{0.5}O_4$ was also confirmed by Mossbauer spectra in a previous work [11]. Therefore, in the initial composition $LiMn_{1.5}Fe_{0.5}O_4$, Mn^{3+} still remains and a Jahn–Teller distortion is expected to occur during the intercalation of a second lithium as observed by XRD.

Fig. 4(a) shows XRD patterns of $LiMnNiO_4$. The pattern could be indexed mainly as a layered rock-salt hexagonal structure with a unit cell parameter $a=2.891$ Å and $c=14.297$ Å similar to the structure of $LiNiO_2$. A spinel structure could also be considered for indexing this pattern because the peaks are broad which make it very difficult to distinguish between these two structures. The reason why we considered the layered rock-salt structure for this material is that the intensity of the Bragg peak situated at $2\theta=43.86°$ is larger than the one observed in the normal spinels. The increase in intensity of this peak is usually observed in the disordered layered rock-salt structure. Furthermore, the diffraction peak situated at $2\theta=63.88°$ is asymmetric and can therefore be deconvoluted to two peaks which could be indexed as the (108) and (110) of the layered structure. In addition the c/a ratio of 4.945 in this case is significantly different from the ratio provided for an ideal cubic unit cell ($c/a=4.899$). Fig. 4(b) shows the XRD pattern of $LiMnFeO_4$. This pattern corresponds to an inverse spinel with the diffraction peak (111) much weaker than the (220) peak and with a unit cell parameter of $a=8.370$Å. In the normal spinel, the (111) peak is the most intense peak in the pattern and the (220) peak is almost inexistent. The reason of the switch in the intensities of these diffraction peaks is the presence of heavier transition metal (probably iron) in the tetrahedral 8*a* site of the inverse spinel in comparison with the normal spinel where only lithium occupies the tetrahedral 8*a* site. This phenomenon leads to the increase in the diffraction response of the (220) peak at the expense of (111) peak.

Fig. 5(a) shows the $Ni2p_{3/2}$ XPS emission spectrum of $LiMnNiO_4$. Only one peak at 855.09 eV associated with a broad satellite peak could be observed. The binding energy of this peak is similar to that observed in $LiNiO_2$ and higher than that observed in $LiMn_{1.5}Ni_{0.5}O_4$ where nickel is divalent. This result indicates that the nickel in this case is trivalent. The shift toward higher binding energy of the XPS peak observed in Ni^{3+} compared with Ni^{2+} could be explained by the difference in the electronic screen effect on the electrons situated at the ($2p_{3/2}$) level in both ions. The electronic screen effect is lower in the case of Ni^{3+} than in Ni^{2+} ion (Ni^{3+} has fewer electrons). As a result, the positive interaction between the nucleus and the electron situated at the $2p_{3/2}$ level increases. Therefore, a higher energy is needed to pull the electron from this level, thus inducing a shift of the corresponding binding energy toward higher level. Fig. 5(b) shows the XPS $Fe2p_{3/2}$ emission spectrum of $LiMnFeO_4$. Only one peak with a binding energy (712.5 eV) similar to that obtained in both Fe_2O_3 and $LiMn_{1.5}Fe_{0.5}O_4$ is observed. This result indicates that the increase in the content of iron doping in the spinel does not affect the oxidation state of iron which remains trivalent in contrast to the nickel-doped materials where the nickel changes from divalent to trivalent after increasing the content of the dopant.

4. Electrochemical investigation

The electrochemical characteristics of nickel- and iron-doped spinel cathodes were evaluated in glass or Teflon-type

cells. Each cell consists of a spinel cathode material, a lithium metal negative electrode, a lithium reference and an electrolyte made either of 1 M $LiClO_4$ + (EC + DEC) or $LiPF_6$ dissolved in sulfolane electrolyte. The cell was charged and discharged at a current density of 0.5 mA/cm^2.

Fig. 6 shows the charge and discharge characteristics of $LiMn_{1.5}Ni_{0.5}O_4$ (Fig. 6(a)) and $LiMn_{1.5}Fe_{0.5}O_4$ (Fig. 6(b)). The nickel-doped material presents a 3 V discharge capacity at around 160 mAh/g and a fairly good cyclic reversibility because of the none structural change during the charge/discharge processes. In this case, the cell was cycled in the voltage limit between 4.2 and 2 V by initially discharging the cell to intercalate a second lithium in $Li_{1+x}Mn_{1.5}Ni_{0.5}O_4$. The absence of the 4 V region in this case is due to the no existence of Mn^{3+} at the initial stage to be oxidized to Mn^{4+} by first charging $LiMn_{1.5}Ni_{0.5}O_4$. However, the iron-doped material presents clearly two plateaus at 4 and 3 V with a sharp voltage drop caused by the structural transition from cubic to tetragonal induced by the Jahn–Teller effect of increasing trivalent manganese ion upon discharging the cell. The material shows also a poor cyclic reversibility because of the structural transition from cubic to tetragonal upon cycling. Fig. 7 shows the first charge and discharge curves of $LiMnNiO_4$. A similar 3 V plateau to that obtained in $LiMn_{1.5}Ni_{0.5}O_4$ is observed with lower capacity. In this case also, the cell was cycled in the voltage limit 4.2–2 V. The 3 V plateau observed in both nickel-doped materials with different composition is caused by the reduction of Mn^{4+} to Mn^{3+} when intercalating a second lithium after initially discharging the corresponding cells. However, lithium could be extracted from these materials ($Li_{1-x}MnNiO_4$ and

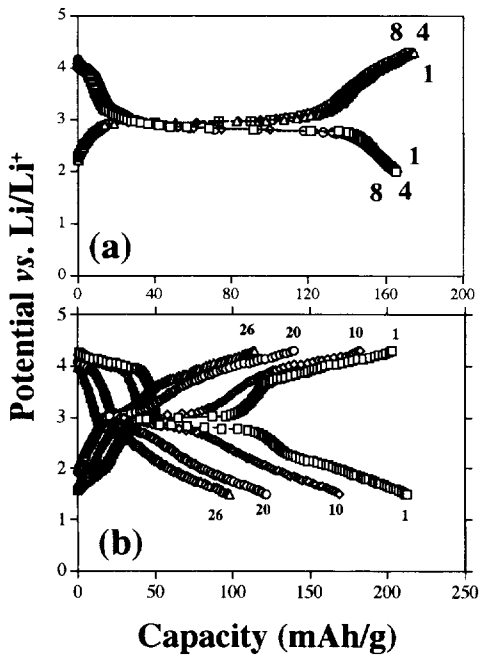

Fig. 6. Charge and discharge curves of: (a) $Li_{1+x}Mn_{1.5}Ni_{0.5}O_4$, and (b) $LiMn_{1.5}Fe_{0.5}O_4$. The test was conducted using 1 M $LiClO_4$ + (EC + DMC + DEC) as the electrolyte at a current density of 0.5 mA/cm^2

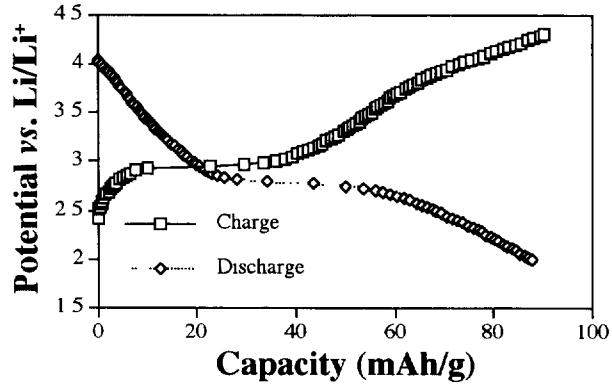

Fig. 7. Charge and discharge curves of $LiMnNiO_4$. The test was conducted using 1 M $LiClO_4$ + (EC + DMC + DEC) as the electrolyte at a current density of 0.5 mA/cm^2.

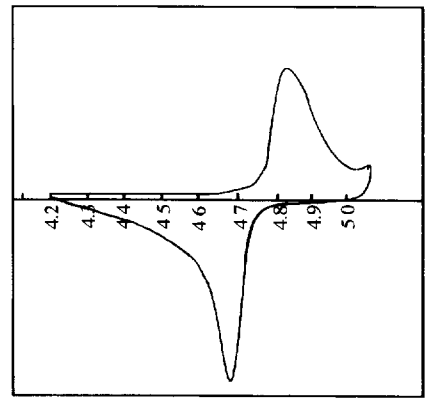

Fig. 8. Cyclic voltammogram of $Li_{1-x}Mn_{1.5}Ni_{0.5}O_4$, scan rate: 0.2 mV/s.

$Li_{1-x}Mn_{1.5}Ni_{0.5}O_4$), if trivalent or divalent nickel could be oxidized to a higher state by removing an electron from Ni3de$_g$ level. This could take place if the cells are initially charged at high voltage of 5 V. Fig. 8 shows the cyclic voltammogram of $LiMn_{1.5}Ni_{0.5}O_4$ in the potential range of 4.2 to 5.1 V. The test was conducted at room temperature using Li/Li^+ as the reference electrode and $LiPF_6$ dissolved in sulfolane as the electrolyte at a scan rate of 0.2 mV/s. The electrolyte used in this case has a wide stability window and can bear up to 5.3 V when charging the cell. Upon cycling, one oxidation and one reduction peak are observed at around 4.7 V. The existence of these two peaks indicates a reversible one-stage process for extracting and intercalating lithium in $Li_{1-x}Mn_{1.5}Ni_{0.5}O_4$. In this case Ni^{2+} is oxidized to Ni^{4+} upon extracting lithium from $Li_{1-x}Mn_{1.5}Ni_{0.5}O_4$. A similar behavior could be observed also for the material $LiMnNiO_4$. Fig. 9 shows the charge and discharge curves during the first cycle of $Li_{1-x}Mn_{1.5}Ni_{0.5}O_4$. The material shows a plateau at around 4.7 V with a discharge capacity of 90 mAh/g still lower than the theoretical one (149 mAh/g) which corresponds to the total oxidation of divalent nickel to the tetravalent state. The material shows also a fairly good cyclic reversibility with very limited loss in capacity after 16 cycles (Fig. 10) due to the fact that the material retains its normal spinel structure

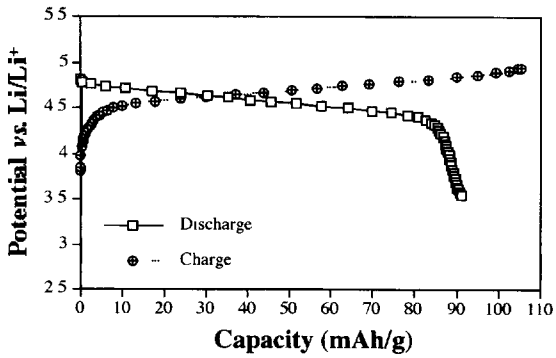

Fig. 9 Charge and discharge curves of $Li_{1-x}Mn_{1.5}Ni_{0.5}O_4$ Test was conducted using 1 M $LiPF_6$ + sulfolane as the electrolyte at a current density of 0.5 mA/cm^2.

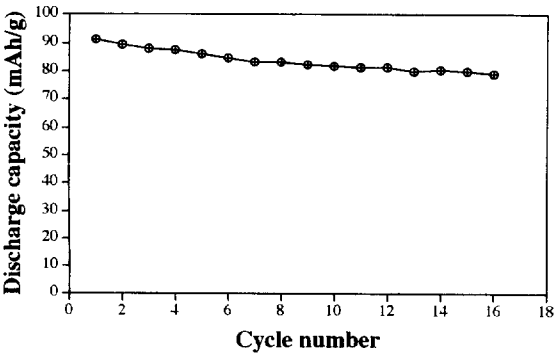

Fig. 10. Discharge capacity vs. cycle number of $Li_{1-x}Mn_{1.5}Ni_{0.5}O_4$. The test was conducted using 1 M $LiPF_6$ + sulfolane as the electrolyte at a current density of 0.5 mA/cm^2.

with a possible presence of free tetrahedral tunnel where lithium could diffuse easily. Such a behavior is different from that of recently reported high voltage spinel $LiNiVO_4$ [12] which shows limited capacity and rather poor cyclability because lithium ions in the tetrahedral tunnels are blocked by the presence of transition metal in the inverse spinel structure. Fig. 11 shows the first charge and discharge curves of $LiMnFeO_4$. The material has an average potential of 1–2 V with a capacity of 120 mAh/g. This result is totally different from inverse spinels $LiNiVO_4$ [12] and $LiMnCrO_4$ [13] where lithium could be extracted and intercalated at 4.8 V.

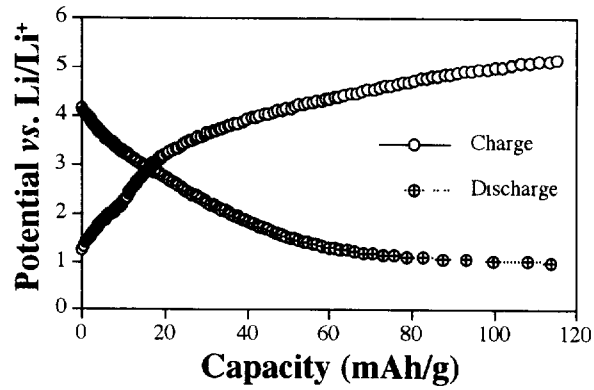

Fig 11. Charge and discharge curves of $LiMnFeO_4$. The test was conducted using 1 M $LiPF_6$ + sulfolane as the electrolyte at a current density used of 0.5 mA/cm^2.

References

[1] T Ohzuku, M. Kitagawa and T. Hirai, *J Electrochem. Soc., 137* (1990) 769.
[2] P. Barboux, J.M. Tarascon and F.K. Shokoohi, *J Solid State Chem., 94* (1991) 185.
[3] M.M. Thackeray, A. DeKok, M.H. Rossouw, D. Liles, R. Bittihn and D. Hoge, *J. Electrochem. Soc., 139* (1992) 363.
[4] J.M Tarascon and D. Guyomard, *J Electrochem. Soc , 138* (1991) 2864.
[5] M.M Thackeray, W I.F. David, P.G. Bruce and J.B. Goodenough, *Mater Res. Bull., 18* (1983) 461.
[6] J M. Tarascon, E. Wang, F.K. Shokoohi, W.R. McKinnon and S. Colson, *J. Electrochem. Soc., 138* (1991) 2859
[7] R. Bittihn, R Herr and D. Hoge, *J. Power Sources, 43–44* (1993) 223.
[8] R.J. Gummow, A. De Kock and M.M. Thackeray, *Solid State Ionics, 69* (1994) 59
[9] K. Amine, H Tukamoto, H Yasuda and Y. Fujita, *J. Electrochem. Soc., 143* (1996) 1608.
[10] C.D. Wagner, W.M. Riggs, L.E. Davis, F.F. Moulder and G E Muilenberg, *Handbook of X-ray Photoelectron Spectroscopy*, Perkin-Elmer, Minneapolis, 1978, pp. 60–100.
[11] C.J. Chen, *J. Solid State Chem., 64* (1986) 240.
[12] G.T. Fey, W. Li and J.R. Dahn, *J. Electrochem. Soc., 141* (1990) 2279
[13] C. Sigal, D Guyomard, A. Verbaere, Y. Piffard and M. Tournoux, *Solid State Ionics, 81* (1995) 167.